

Purely entropy-driven magnetic phase transitions in the kagomé system volborthite

Myung-Hwan Whangbo^{a,b,*}, Hyun-Joo Koo^b, Eva Brücher^c, Pascal Pupal^c, and Reinhard K. Kremer^{c,*}

^a Department of Chemistry, North Carolina State University, Raleigh, NC 27695-8204, USA

^b Department of Chemistry and Research Institute for Basic Sciences, Kyung Hee University, Seoul 02447, Republic of Korea

^c Max Planck Institute for Solid State Research, Heisenbergstrasse 1, D-70569 Stuttgart, Germany

Abstract

The magnetic properties of volborthite, $\text{Cu}_3\text{V}_2\text{O}_7(\text{OH})_2 \cdot 2\text{H}_2\text{O}$, possessing kagomé layers of Cu^{2+} (d^9 , $S=1/2$) ions, were examined by measuring the magnetic susceptibilities and the specific heats of $\text{Cu}_3\text{V}_2\text{O}_7(\text{OH})_2 \cdot 2\text{H}_2\text{O}$ and $\text{Cu}_3\text{V}_2\text{O}_7(\text{OD})_2 \cdot 2\text{D}_2\text{O}$ under magnetic fields $B = 0 - 9$ T and also by evaluating the spin exchanges for the $I2/a$ and $P2_1/a$ structures of volborthite using DFT calculations. We demonstrate that the low-temperature magnetic properties of volborthite are very well described by a $S=1/2$ antiferromagnetic uniform Heisenberg (AUH) chain model in stark contrast to earlier theoretical reports that suggested a Heisenberg triangular lattice made up of $S=1/2$ pseudospin units. The spin exchanges of volborthite determined from our work show that each kagomé layer consists of two-leg spin ladders with rungs of $S=1/2$ pseudospin units, and these rungs couple to form a $S=1/2$ AUH chain responsible for the observed low-temperature magnetic properties. The two specific heat anomalies of volborthite below 1.5 K, representing the magnetic ordering within and between kagomé layers of volborthite, are suppressed by a magnetic field of

~ 4.2 T, but a new specific heat anomaly occurs under magnetic field higher than ~ 5.5 T. We find that possible spin arrangements of antiferromagnetically-coupled spin ladders give rise to three sets of entropy spectra identical in enthalpy due to the topologically-constrained interactions between adjacent two-leg spin ladders in each kagomé layer, and that these three magnetic entropy spectra explain both the suppression of the specific anomalies by magnetic field of ~ 4.2 T and the emergence of a new specific anomaly by magnetic field above ~ 5.5 T. These observations strongly support that the specific heat anomalies of volborthite below 1.5 K and their dependence on applied magnetic field are driven by magnetic entropy, and predict that the specific heat anomaly occurring under magnetic field above ~ 5.5 T will disappear under magnetic field probably higher than ~ 13 T. The entropy-driven nature of the specific anomalies below 1.5 K is further supported by the observation that the effect of the isotope exchange H \rightarrow D on the specific heat anomalies below 1.5 K is very weak compared with that on the structural phase transition temperature from the $I2/a$ to the $P2_1/a$ structure.

1. Introduction

Antiferromagnets possessing a kagomé arrangement of transition-metal magnetic ions M are often expected to suppress a long-range magnetic order thereby leading to spin liquids.^{1,2} However, it is not at all rare to find that such systems rather exhibit a long-range order or a glass-like behavior at sufficiently low temperatures, which may arise, e.g., from quenched disorder or symmetry lowering by structural phase transitions. In fact, spin frustration is not guaranteed per se by a trigonal, a kagomé or a pyrochlore structural arrangement of magnetic ions M , in particular, for transition-metal magnetic ions which, unlike rare-earth cations, interact strongly with the surrounding main-group ligands L to form ML_n polyhedra. What is crucial for geometrical spin frustration is not the geometrical arrangement of magnetic ions M , but that of the spin exchanges they develop between their neighbors. Spin exchanges between magnetic ions M are determined by their magnetic orbitals, namely, the singly-occupied d -states of their ML_n polyhedra.^{3,4} The d -states have the d -orbitals of M combined out of phase with the p -orbitals of the ligands L , so they are not isotropic in shape. Consequently, even if the magnetic ions form a kagomé structural arrangement, the spin exchanges between magnetic ions do not necessarily form the same pattern. This is a consequence of the anisotropy effect of magnetic orbitals and most strongly felt for a magnetic ion possessing one magnetic orbital (e.g., Cu^{2+}), and least strongly felt for a magnetic ion with five magnetic orbitals (e.g., high-spin Mn^{2+} and high-spin Fe^{3+} ions).

A system that lately came into focus is volborthite,⁵⁻¹¹ $Cu_3V_2O_7(OH)_2 \cdot 2H_2O$, the crystal structure of which is characterized by slightly distorted kagomé layers of Cu^{2+} (d^9 , $S = 1/2$) cations occupying two different crystallographic sites in a ratio 2:1. Below room temperature, each Cu^{2+} ion forms an axially-elongated CuO_6 octahedron so that, with the local z -axis taken along the elongated $Cu-O$ bonds, the magnetic orbital of each CuO_6 octahedron is the x^2-y^2 state contained in the CuO_4 equatorial plane, which is quite anisotropic in shape. In volborthite, the kagomé layers

of composition $\text{Cu}_3\text{O}_6(\text{OH})_2$ parallel to the ab -plane are pillared by pyrovanadate groups V_2O_7 , and the voids between the layers provide space for crystal water molecules. Below room temperature volborthite undergoes two structural phase transitions, one at ~ 292 K from a phase described by the space group $C2/c$ to $I2/a$, and the other at about ~ 155 K from the $I2/a$ phase to another monoclinic phase described by the space group $P2_1/c$.⁶ The latter structural phase transition generates two different kagomé layers, which are slightly different in structure. Below 1.5 K volborthite exhibits magnetic order indicated by two anomalies in the magnetic specific heat. On the basis of their DFT+U calculations, Janson *et al.* described the magnetic properties of volborthite using a trigonal spin lattice composed of pseudo $S=1/2$ units, i.e., linear spin trimers in which adjacent Cu^{2+} ions are strongly coupled antiferromagnetically.¹¹ However, the nature of the magnetically ordered states below 1.5 K remained unclear. Another striking aspect of the reported magnetic property of volborthite is that its susceptibility is nonzero as the temperature is decreased toward 0 K,⁵ which is a well-known characteristic, e.g., of a $S=1/2$ A1H chain. However, the magnetic susceptibility Janson *et al.* calculated for volborthite by exact diagonalization of the spin Hamiltonian using the trigonal lattice composed of pseudo $S=1/2$ units exhibits a precipitous decrease below the maximum, in disagreement with the experimental observation.

To explore the magnetic order below 1.5 K, especially its magnetic field dependence, as well as the origin of the apparently finite susceptibility as $T \rightarrow 0$ K, we re-analyze the spin lattice of volborthite by performing an energy-mapping analysis based on DFT+U calculations, to find that the magnetic properties of volborthite below 75 K should be described by two-leg spin ladders with rungs made up of $S=1/2$ pseudospin units, i.e., the linear trimers identified by Janson *et al.* We verify this conclusion by analyzing new data and re-analyzing reported magnetization data of volborthite to find that the low-temperature ($T \lesssim 75$ K) magnetic properties of volborthite are

indeed well described by a $S=1/2$ AUH chain composed of $S=1/2$ rung-pseudospins. To characterize the magnetic phase transitions below 1.5 K, we carry out specific heat measurements for $\text{Cu}_3\text{V}_2\text{O}_7(\text{OH})_2 \cdot 2\text{H}_2\text{O}$ and its deuterated analogue, $\text{Cu}_3\text{V}_2\text{O}_7(\text{OD})_2 \cdot 2\text{D}_2\text{O}$, under high magnetic field to discover that volborthite undergoes magnetic-field-induced re-entrant ordering below 1.5 K and show that this magnetic ordering arises from topologically-constrained interactions between the two-leg spin ladders in each kagomé layer of Cu^{2+} ions and is hence purely entropy-driven.

2. Experimental and calculations

Single crystals of volborthite were grown using hydrothermal techniques as described in the literature.⁶ Deuterated samples of volborthite were prepared by replacing light by heavy water (isotope enrichment 99.5 %). The magnetic susceptibilities were measured at constant field as a function of the temperature in a Magnetic Property Measurement System SQUID magnetometer (MPMS-XL7, Quantum Design). The specific heats of a collection of oriented crystals were determined using the relaxation method of a 3-He Physical Property Measurement System (PPMS, Quantum Design). In order to construct a lattice reference needed to evaluate the magnetic contribution to the specific heat of volborthite, we prepared a polycrystalline sample of the diamagnetic mineral martyite with composition $\text{Zn}_3\text{V}_2\text{O}_7(\text{OH})_2 \cdot 2\text{H}_2\text{O}$ from an aqueous solution of NH_4VO_3 and zinc acetate, $\text{Zn}(\text{CH}_3\text{CO}_2)_2$, following a recipe reported in the literature.¹²

To determine the spin exchanges of the $I2/a$ and $P21/c$ phases of volborthite, we carry out DFT+U calculations employing the Vienna ab Initio Simulation Package (VASP)^{13,14} using the projector augmented wave (PAW)^{15,16} method and the PBE¹⁷ exchange-correlation functional. The electron correlation associated with the 3d states of Cu was taken into consideration by DFT+U

calculations, i.e., by performing DFT calculation with an effective on-site repulsion $U_{\text{eff}} = U - J = 4$ and 5 eV added on the magnetic ions Cu^{2+} .¹⁸

4. Results and Discussion

4.1. Spin exchanges and spin lattice of volborthite

We determine the relevant spin exchanges $J_1 - J_5$ defined in **Figure 1a** by performing the energy-mapping analyses^{3,4} based on DFT+U calculations (for details of calculations, see the Supplemental Material, SM). Below room temperature down to ~ 155 K, volborthite has a crystal structure with two equivalent kagomé layers in the unit cell (space group the $I2/a$) phase and below 155 K a structure with two slightly nonequivalent kagomé layers of Cu^{2+} ions (space group $P2_1/a$).^{5,8} The spin exchanges of the two phases are very similar as summarized in **Table 1**, where only the values obtained with $U_{\text{eff}} = 4$ eV are listed. Those calculated with $U_{\text{eff}} = 5$ eV are given in the SM. Janson *et al.*¹¹ carried out DFT+U calculations using $U_{\text{eff}} = 8.5, 9.5$ and 10.5 eV to determine the spin exchanges of the $P2_1/a$ structure by fitting the electronic band structure in terms of a tight binding approximation. For the purpose of comparison, the values of their spin exchanges obtained by using $U_{\text{eff}} = 8.5$ eV are also listed in **Table 1**. In the following we first discuss the spin lattice of volborthite suggested by the spin exchanges we obtained. Subsequently, we show that the same picture is obtained from those of Janson *et al.*, and that their spin exchanges are considerably smaller than ours in the strengths of AFM character due to their use of very large U_{eff} values.

As can be seen from **Table 1**, the strongest exchange J_2 is AFM and it forms isolated linear trimers (**Figure 1a**). The second strongest spin exchange J_4 is also AFM but is weaker than J_2 by nearly an order of magnitude. All other spin exchanges are weaker than J_2 by more than an order

of magnitude. Since J_2 is much stronger than other spin exchanges, each linear trimer at $T \ll J_2$ constitutes a pseudospin $S=1/2$ unit and such units form a triangular lattice, as already described by Janson *et al.*¹¹ However, we note that the linear trimers interact through the exchange J_4 to form two-leg spin ladders with the linear trimers as rungs (**Figure 1b**). This feature is hidden in a kagomé layer because all nearest-neighbor spin ladders are geometrically entangled with their superposed legs.

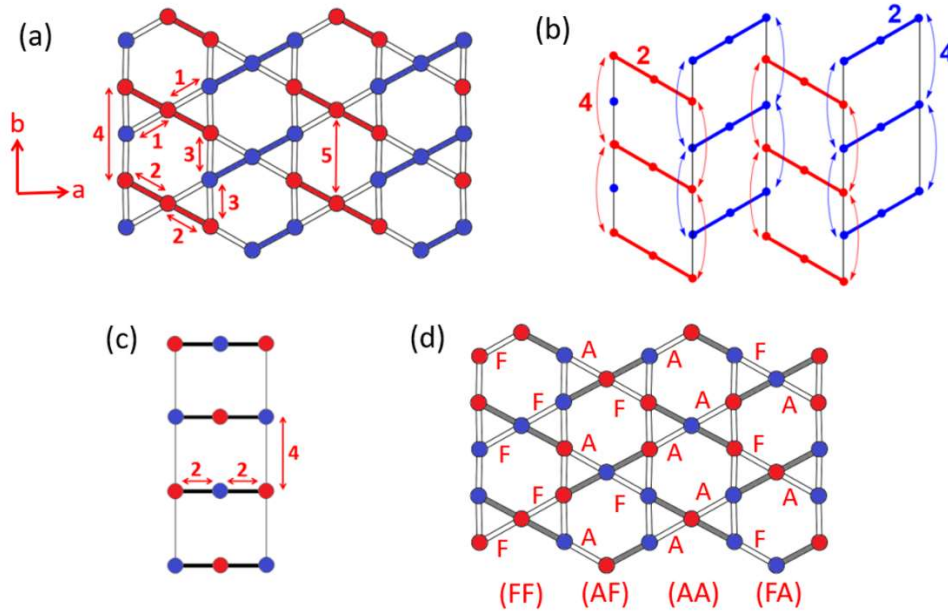


Figure 1. (a) The kagomé arrangement of Cu^{2+} ions (red and blue circles) in volborthite, where the labels 1 – 5 refer to the spin exchanges $J_1 – J_5$, respectively (see **Table 1**). In each J_2 path, two Cu^{2+} ions make a $\text{Cu-O}\dots\text{V}^{5+}\dots\text{O-Cu}$ bridge, while the remaining exchange paths do not. (b) Geometrical entanglement of adjacent two-leg spin ladders in a kagomé layer. Adjacent spin ladders are presented with different colors for ease of distinction. (c) A two-leg spin ladder with rungs of linear trimers defined by J_2 and legs defined by J_4 , with all exchange paths antiferromagnetically coupled, where the red and blue circles represent the up-spin and down-spin Cu^{2+} ion sites, respectively. (d) A spin ladder arrangement in which (FF)-, (AF)-, (AA)- and (FA)-coupled spin ladders occur consecutively.

Janson *et al.*'s spin exchanges (**Table 1**) are also in support of the two-leg spin ladder model as the spin lattice of volborthite described above. However, their spin exchanges differ

considerably from ours in magnitude. In general, a spin exchange J between two magnetic ions located at sites i and j can be written as the sum of the FM and AFM components (J_F and J_{AF} , respectively), namely, $J = J_F + J_{AF}$.^{3,4,19} With the magnetic orbitals describing the spin sites i and j as ψ_i and ψ_j , respectively, the overlap density $\rho_{ij} = \psi_i\psi_j$ gives rise to the exchange repulsion K_{ij} while the overlap integral $\langle\psi_i|\psi_j\rangle$ leads to an energy split Δe between the two states described by the magnetic orbitals. Then, J_F and J_{AF} are written as

$$J_F = -K_{ij}, \text{ and } J_{AF} = \frac{(\Delta e)^2}{U_{\text{eff}}} \quad (1)$$

Note that the AFM component J_{AF} is inversely proportional to U_{eff} , predicting that use of a large

Table 1. Values (in K) of the spin exchanges $J_1 - J_5$ calculated for the $I2/a$ and $P2_1/a$ phases of volborthite obtained by DFT+U calculations

$I2/a$ phase ^a		$P2_1/a$ phase ^a		$P2_1/a$ phase ^b	
		Layer 1	Layer 2	Layer 1	Layer 2
J_1/J_2	0.010	-0.001	-0.025	-0.15	-0.11
J_3/J_2	0.025	0.031	0.031	-0.34	-0.32
J_4/J_2	0.145	0.141	0.135	0.17	0.15
J_5/J_2	0.014	0.014	0.013	-	-
J_2	542 K	550 K	582 K	193 K	205 K

^a Present work with $U_{\text{eff}} = 4$ eV

^b Janson *et al.* (ref. 11) with $U_{\text{eff}} = 8.5$ eV.

U_{eff} value in DFT+U calculations should make J value less strongly AFM or even FM. This explains why the J_2 and J_4 values of Janson *et al.* are less strongly AFM than ours, and why their J_1 and J_3 values are more strongly FM than ours.

Within each AFM exchange path J_4 , there occur two consecutive J_3 exchanges (**Figure 1a**), but the effects of the J_3 exchanges within each J_4 AFM path cancel out regardless of whether J_3 is ferromagnetic FM or AFM. Therefore, adjacent spin ladders interact only through the very weak exchanges J_1 (**Figure 1a**). Note that J_1 is weakly AFM for the $I2/a$ phase, but is weakly FM for the $P2_1/a$ phase in our calculations. This difference does not matter how the ordering between spin ladders in a kagomé layer is affected by J_1 (see below). Since J_1 is more than an order of magnitude weaker than J_4 , the magnetic property of each kagomé layer at low temperatures ($|J_1| < T \ll J_2$) is determined by those of the spin ladders with each linear trimer acting as an effective $S=1/2$ pseudospin rung (**Figure 1c**). The dominant AFM spin exchanges leading to the two-leg ladders predict that volborthite should possess a $S=1/2$ AUH chain behavior at low temperature with no sign of spin frustration, so that a $S=1/2$ AUH chain model is more appropriate than the triangular lattice model composed of pseudo-spin $1/2$ units.

4.2. Evidence for the spin-half antiferromagnetic uniform Heisenberg chain character

Figure 2 displays the magnetic susceptibilities of volborthite, which exhibits a broad peak at ~ 17 K and a finite susceptibility as $T \rightarrow 0$ K characteristic of a low-dimensional AFM short range order (SRO) behavior. As implied by the results of the DFT+U calculations the magnetic susceptibilities of volborthite between 3 and 75 K can indeed be very well fitted by those theoretically predicted for a $S=1/2$ AUH chain according to

$$\chi_{\text{mol}}(T) = (1 - x_{\text{imp}})\chi_{\text{spin}}(J_C, g, T) + \chi_0 \quad (2)$$

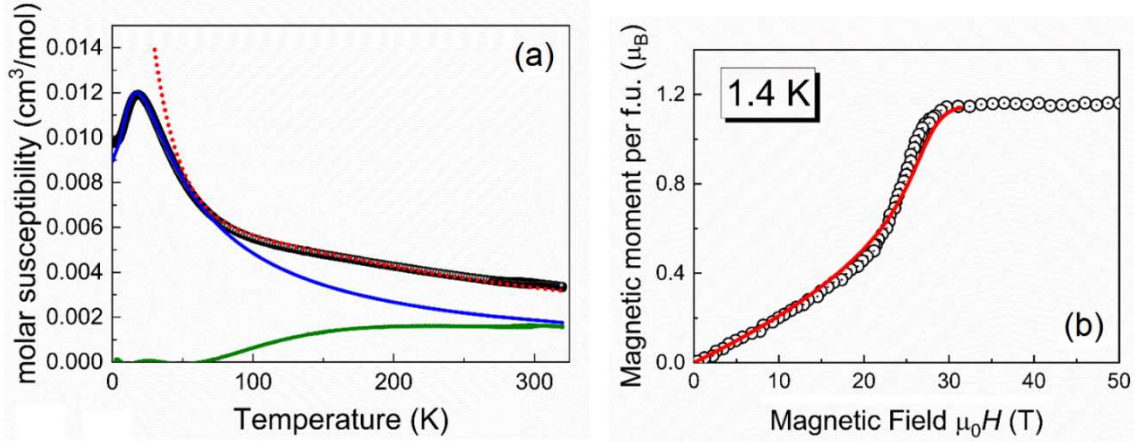


Figure 2. (a) The magnetic susceptibility of one formula unit (i.e., comprising three Cu atoms) of volborthite (black circles) with H applied along the crystallographic b axis fitted (for $T < 75$ K) to the theoretical prediction for a $S=1/2$ AUH chain (solid blue curve). The difference between the two is displayed as a solid green line. The experimental susceptibilities for $75 \text{ K} \leq T \leq 320 \text{ K}$ are well fitted by the susceptibility of a linear spin $S=1/2$ trimer with spin exchange of $197(\text{K})$ (red dotted curve). Note the susceptibility anomaly at $\sim 295 \text{ K}$ due to the structural phase transition from the $C2/c$ to the $I2/a$ phase.⁵ (b) Isothermal magnetization of volborthite determined at 1.4 K taken from ref. 11. compared with quantum Monte Carlo calculations for a $S=1/2$ AUH chain with a spin exchange of $J_C = 27.5 \text{ K}$ (solid red line).

where $\chi_{\text{spin}}(J_C, g, T)$ represents the magnetic susceptibility of the $S=1/2$ AUH chain with nearest-neighbor (NN) spin exchange J_C (**Figure 2a**). For $\chi_{\text{spin}}(J_C, g, T)$ we use the Padé approximant of Quantum Monte Carlo (QMC) results for the $S=1/2$ AUH chain.²⁰ The second term refers to the temperature-independent susceptibility χ_0 arising from the diamagnetism of the electrons in the closed shells ($-175 \times 10^{-6} \text{ cm}^3/\text{mol}$ per FU)^{21,22} and also from the van Vleck paramagnetic susceptibility due to excitations to the excited states of each Cu^{2+} ion ($\sim 100 \times 10^{-6} \text{ cm}^3/\text{mol}$ per Cu atom),²³ leading to $\chi_0 = +125 \times 10^{-6} \text{ cm}^3/\text{mol}$ per FU. Up to $\sim 75 \text{ K}$ the experimental susceptibility is well reproduced by the susceptibility calculated for a $S=1/2$ AUH chain with $J_C = 27.8(5) \text{ K}$ and

$g = 2.33$ (the solid blue curve in **Figure 2a**). The fitted g-factor is found to be 2.33, which is at the higher end of the g-factor expected for Cu^{2+} ions.²⁴ The S=1/2 AUH chain model readily explains the susceptibility maximum at $T_{\text{max}} = 17$ K as well as the finite susceptibility below T_{max} . The exchange $J_C = 27.8(5)$ K agrees very well with the expected value $J_C = T_{\text{max}}/0.64085 = 26$ K. In addition, the ratio $\chi_{\text{max}}T_{\text{max}}/g^2 = 0.0346$ cm³ K/mol concurs well with the value 0.0353 expected for the S=1/2 AUH chain.²⁰ The difference between the experimental data and the chain susceptibility (green solid line in **Figure 1**) vanishes below ~ 75 K and gradually increases to higher temperatures. The susceptibilities above ~ 75 K without any constraints matches very well with the susceptibility of an isolated linear spin S=1/2 trimer described by the spin Hamiltonian

$$\mathcal{H} = J_{\text{trim}} (\vec{S}_1 \cdot \vec{S}_2 + \vec{S}_2 \cdot \vec{S}_3), \quad (3)$$

where \vec{S}_i ($i = 1, 2, 3$) represent the three spin sites. Replacing $\chi_{\text{spin}}(J, g, T)$ in eq. (2) with the susceptibility of a spin S=1/2 trimer given, e.g., by Boukhari *et al.*²⁵ the susceptibility data above ~ 75 K can be well fitted without further constraints. The trimer spin exchange amounts to 197(2) K, indicating a ratio $J_C/J_{\text{trim}} = 0.14$, in good agreement with the ratio J_4/J_2 obtained from our DFT+U calculation (see **Table 1**) suggesting that the spin trimers should be identified as the rungs of the two-leg spin ladders running along the crystallographic b axis.

Another characteristic feature of the magnetic properties of volborthite is the low-temperature 1/3 magnetization plateau extending over a wide magnetic field range, displayed in **Figure 2b**.^{8,9} Multiplying the published literature data by a factor of three to obtain the magnetization per FU of volborthite (3 Cu atoms), the experimental data are well reproduced by the magnetization predicted for the S=1/2 AUH chain with $J_C = 27.5$ K. The theoretical magnetization was obtained by Quantum Monte Carlo Calculations (QMC) employing the path integral method of the loop code incorporated within the ALPS project.^{26,27} To ensure a low

statistical error, these simulations included 250 spins and 1.5×10^5 Monte Carlo steps for the initial as well as a subsequent thermalization.

4.3. Specific heat anomalies and magnetic order

In **Figure 3a**, we show the specific heat measured for an ensemble of aligned volborthite crystals in zero magnetic field with magnetic field applied along the b axis, the estimated lattice contribution to the heat capacity constructed from the specific heat of $\text{Zn}_3\text{V}_2\text{O}_7(\text{OH})_2 \cdot 2\text{H}_2\text{O}$,²⁸ and the difference between the two representing the magnetic contribution to the specific heat of volborthite. As already pointed out by Yamashita *et al.*,¹⁰ it is difficult to obtain a proper lattice specific heat reference because the atomic masses of Cu and Zn are not the same and because the space groups describing the crystal structures of $\text{Zn}_3\text{V}_2\text{O}_7(\text{OH})_2 \cdot 2\text{H}_2\text{O}$ ($P\bar{3}m1$) and $\text{Cu}_3\text{V}_2\text{O}_7(\text{OH})_2 \cdot 2\text{H}_2\text{O}$ ($I2/a$ and $P2_1/a$) are different. In our work, we adopt the procedure suggested by Boo and Stout²⁹ and stretch the temperature axis of the specific heat data for $\text{Zn}_3\text{V}_2\text{O}_7(\text{OH})_2 \cdot 2\text{H}_2\text{O}$ with a smooth function varying from 1.15 at 0 K to 1.05 at 50 K. The latter values were chosen such that the specific heat of $\text{Zn}_3\text{V}_2\text{O}_7(\text{OH})_2 \cdot 2\text{H}_2\text{O}$ smoothly approaches that of volborthite as $T \rightarrow 50$ K. The magnetic specific heat of volborthite thus obtained exhibits a broad maximum consistent with the specific heat capacity expected for a $S=1/2$ AUH with a NN spin exchange of $J_C = 26$ K. The latter value is in good agreement with the spin exchanges derived from the analyses of the magnetic susceptibility and magnetization data. The total magnetic entropy amounts to $\sim 80\%$ of $R \ln 2$ expected for a $S=1/2$ system, consistent with the result reported by Yamashita *et al.*¹⁰ In **Figure 3b**, we compare the specific heats of $\text{Cu}_3\text{V}_2\text{O}_7(\text{OH})_2 \cdot 2\text{H}_2\text{O}$ and its deuterated analogue, $\text{Cu}_3\text{V}_2\text{O}_7(\text{OD})_2 \cdot 2\text{D}_2\text{O}$, prepared by using 99.5 % isotope enriched heavy water. Whereas the magnetic anomalies below 1.5 K (see inset **Figure 3b**) exhibit marginal to no response after the

deuteration, the structural phase transition from $C2/c$ to $I2/a$ near 155 K undergoes a 5 % upshift for the deuterated sample. This is in support of our argument that the two specific heat anomalies below 1.2 K are related to magnetic ordering. Apparently, the $D \rightarrow H$ substitution does not essentially modify the spin exchange between adjacent kagomé layers but substantially affects the structural properties of volborthite. The latter finding reflects the fact that the pyrovanadate groups connecting neighboring kagomé layers effect a large space between them. The hydrogen bond network from an OH group of a kagomé layer to a crystal water to an O atom of the adjacent kagomé layer is loosened by the $D \rightarrow H$ substitution, which facilitates the $I2/a$ to $P2_1/a$ structural transition in $\text{Cu}_3\text{V}_2\text{O}_7(\text{OD})_2 \cdot 2\text{D}_2\text{O}$.

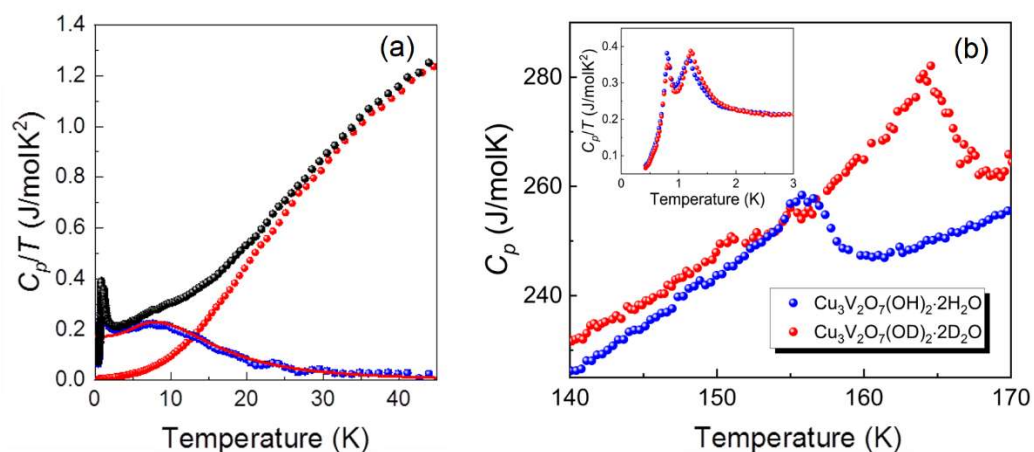


Figure 3. (a) Specific heats of volborthite (black dots) and martyrite, $\text{Zn}_3\text{V}_2\text{O}_7(\text{OH})_2 \cdot 2\text{H}_2\text{O}$ (red dots). The latter was scaled as described in detail in the text to smoothly approach the heat capacity of volborthite at high temperatures. The difference (blue dots) representing the magnetic contribution to the specific heat of volborthite. The solid red line displays the heat capacity of a $S=1/2$ AUH with spin exchange of 26 K and spin entropy amounting to $\sim 80\%$ of $R \ln 2$ expected for a $S=1/2$ system. (b) Comparison of the specific heats of $\text{Cu}_3\text{V}_2\text{O}_7(\text{OH})_2 \cdot 2\text{H}_2\text{O}$ and $\text{Cu}_3\text{V}_2\text{O}_7(\text{OD})_2 \cdot 2\text{D}_2\text{O}$.

4.3. Entropy-driven magnetic phase transitions

A. Re-entrant magnetic ordering

We now examine the nature of the two specific heat anomalies below 1.5 K. These anomalies arise from magnetic ordering. We assign the one at $T_{M1} \approx 1.17$ K to a two-dimensional (2D) short range order within each kagomé layer facilitated by the spin exchange J_1 , and the one at $T_{M2} \approx 0.82$ K to ordering between the 2D-ordered kagomé layers leading to a three-dimensional (3D) magnetic structure. If this speculation is correct, the two anomalies should disappear under strong-enough external magnetic field B . Thus, we carried out specific heat measurements of volborthite under magnetic fields $B = 0 - 9$ T. As B increases, the two specific heat anomalies observed at $B = 0$ grow into separate ridges in the C_p/T plot as a function of T and B , which eventually merge into one and then quickly disappear when $B > \sim 4.2$ T (**Figure 4a**). To our surprise, however, a new anomaly occurs when $B > \sim 5.5$ T, which forms a single ridge broadening and shifting to higher temperatures with increasing B . In what follows, we examine the cause for this re-entrant specific heat anomalies induced by magnetic field.

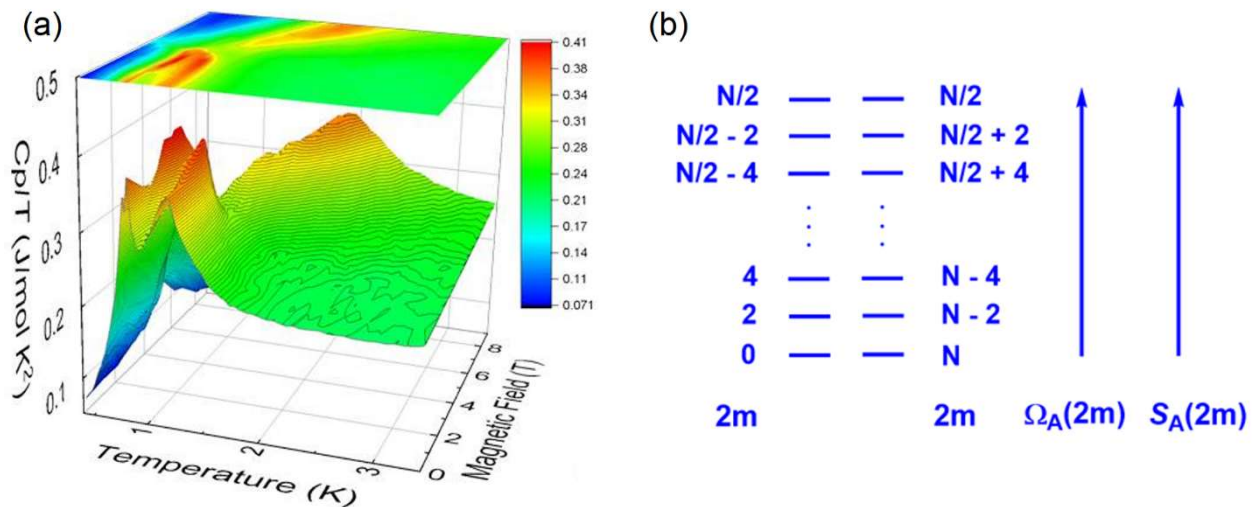


Figure 4. (a) Magnetic field dependence of the specific heat measured with an external magnetic field applied B along the b axis of the volborthite crystals. (b) The spectra of $\Omega_A(2m)$ and $S_A(2m)$ in a kagomé layer of N spin ladders containing m pairs of (AA)- and (FF)-coupled spin ladders. $S_A(2m)$ is the entropy associated with $\Omega_A(2m)$, namely, $S_A(2m) = k_B \ln \Omega_A(2m)$.

B. Magnetic entropy spectra

It is unlikely that, below 1.5 K, the specific heat anomalies of volborthite originate from either the electronic or the vibrational spectra of volborthite, i.e, from the enthalpy spectra of volborthite. Thus, we turn our attention to the magnetic entropy spectra of volborthite and consider the possibility of entropy-driven magnetic phase transitions. Prevailing entropy-driven transitions have been considered to play a role for phase changes in soft matter.³⁰⁻³³ Purely entropy-driven phase transitions were discussed first by Onsager in his theoretical study of nematic phase transition in a system of thin rods,³⁴ but crystalline solids exhibiting such phase transitions are not known although largely entropy-driven cases have been suggested.^{35,36}

For volborthite we put forward the picture that the highly one-dimensionally ordered two-leg spin ladders (hereafter, referred to as spin ladder for short) interact with their neighbors via the spin exchange J_1 to establish 2D correlations within the kagomé layers as a prerequisite for a 3D order at low temperatures. The interactions between adjacent spin ladders are topologically constrained, which has far reaching implications. To begin with, we examine what kinds of arrangements are possible between adjacent two-leg spin ladders within a kagomé layer. Adjacent spin ladders are geometrically entangled via their superposed legs so that there is a topological constraint on the ordering of spin ladders in each kagomé layer. Below 1.5 K where the specific heat anomalies indicated 2D and 3D order, all J_2 and J_4 exchange paths of a spin ladder should be

antiferromagnetically coupled (**Figure 1c**). Two consecutive exchanges J_1 crossing each linear spin trimer of a given spin ladder can be both AFM, both FM, FM and AFM, or AFM and FM, as illustrated in **Figure 1d** where such spin ladders are labeled as the (AA)-, (FF)-, (FA)- and (AF)-coupled spin ladders. It is convenient to use the notation (FF)(AF)(AA)(FA) to represent the consecutive occurrence of (FF)-, (AF)-, (AA)- and (FA)-coupled spin ladders. On crossing each boundary between NN spin ladders, the two sets of J_1 paths close to the boundary should be opposite in the sign of spin exchange so as to keep all exchange paths of every spin ladder antiferromagnetically-coupled. Consequently, (FF)- and (AA)-coupled spin ladders must alternate in a kagomé layer even if they are placed with unequal intervals. Due to this constraint on the spin ladder ordering, there occur only three sets of spin ladder arrangements: Group A with m ($= 0, 1, 2, 3, \dots$) pairs of (AA)- and (FF)-coupled spin ladders in each kagomé layer. Group B (Group C) is the same as Group A except that it has one additional (AA)-coupled [(FF)-coupled] spin ladder. With m, n, o, p, q and r as integers, the spin ladder arrangements of Groups A, B and C can be written as

$$\text{Group A: } (AF)_m(AA)(FA)_n(FF)(AF)_o(AA)(FA)_p(FF)(AF)_q.$$

$$\text{Group B: } (AF)_m(AA)(FA)_n(FF)(AF)_o(AA)(FA)_p(FF)(AF)_q(AA)(FA)_r.$$

$$\text{Group C: } (FA)_m(FF)(AF)_n(AA)(FA)_o(FF)(AF)_p(AA)(FA)_q(FF)(AF)_r.$$

The relative enthalpies of different members in Group A, B or C are solely determined by how many AFM- and FM-coupled J_1 paths are present, because their spin ladders are identical. All possible spin ladder arrangements of Group A are identical in enthalpy (say, $H_A = 0$ per kagomé layer). Similarly, all spin ladder arrangements of Group B are identical in enthalpy, $H_B = H_A - 2J_1 = -2J_1$ per kagomé layer, and those of Group C are identical in enthalpy, $H_C = H_A + 2J_1 = +2J_1$ per kagomé layer (Note that J_1 is weakly FM in the $P21/a$ phase, see **Table 1**). Groups B and C differ

from Group A only in one spin ladder out of the whole spin ladders present in a kagomé layer, and J_1 is very small. Thus, for all practical purposes, $H_A = H_B = H_C$ per kagomé layer.

To probe the entropy spectra of Groups A, B and C, we consider that a kagomé layer has N spin ladders, where $N = N_A/3$ per FU of volborthite $\text{Cu}_3\text{V}_2\text{O}_7(\text{OH})_2 \cdot 2\text{H}_2\text{O}$ with N_A as Avogadro's number. The factor $1/3$ takes into account that each spin ladder has three Cu^{2+} ions per repeat unit. For the case when there are m pairs of (AA)- and (FF)-coupled spin ladders, the total number of different spin ladder arrangements, $\Omega_A(2m)$, in Group A, is given by

$$\Omega_A(2m) = 2({}_N C_{2m}) = 2(N!)/[(2m)!(N-2m)!],$$

where ${}_N C_{2m}$ is the binomial expansion coefficient, and the factor 2 arises because the m pairs of sites in each arrangement can be occupied first with a (FF)-spin ladder or first with an (AA)-coupled spin ladder when $m > 0$. For $m = 0$, $\Omega_A(0) = 2$ because one can have the $(\text{AF})_\infty = \dots(\text{AF})(\text{AF})(\text{AF})\dots$ or the $(\text{FA})_\infty = \dots(\text{FA})(\text{FA})(\text{FA})\dots$ arrangement. The corresponding numbers for Group B (Group C) are given by

$$\Omega_B(2m) = \Omega_C(2m) = \Omega_A(2m) \Omega_E(2m),$$

where $\Omega_E(2m)$ represents the number of possible sites available for an extra spin ladder after m pairs of (AA)- and (FF)-coupled spin ladders are chosen from N spin ladders. Due to the topological constraint on the spin ladder ordering, $\Omega_E(2m) \leq N - 2m$. Then the entropies associated with the three groups of spin ladder arrangements are given by

$$S_A(2m) = k_B \ln \Omega_A(2m),$$

$$S_B(2m) = S_C(2m) = S_A(2m) + S_E(2m),$$

$$S_E(2m) = k_B \ln \Omega_E(2m).$$

Since $\Omega_A(2m) = \Omega_A(N - 2m)$, $\Omega_A(2m)$ increases as $2m$ increases from 0 toward $N/2$, reaching a maximum at $2m = N/2$, and decreases as $2m$ increases beyond $N/2$ toward N (**Figure 4b**).

Consequently, $S_A(2m) = S_A(N - 2m)$, and $S_A(2m)$ increases as $2m$ increases from 0 toward $N/2$ and as $2m$ decreases from N toward $N/2$.

The kagomé layers of volborthite satisfy the three conditions necessary for a crystalline solid to exhibit a purely entropy-driven phase transitions: (1) It has a set of states identical in enthalpy H . (2) The members of this set are grouped into subsets $i = 1, 2, 3, \dots$, with degeneracies $\Omega_1, \Omega_2, \Omega_3, \dots$, respectively. (3) The degeneracy Ω_i increases steadily, e.g., $\Omega_1 < \Omega_2 < \Omega_3 < \dots$, so the associated entropy increases steadily. So one may expect that already moderate magnetic fields inducing Zeeman energies comparable to J_1 are able to substantially alter the entropy balance causing dramatic effects on the low-temperature ordering behavior. In fact, as shown **Figure 4a**, the specific heat anomalies observed at $B = 0$ indeed disappears for $B > \sim 4.2$ T, but a new anomaly occurs when $B > \sim 5.5$ T. Below ~ 2 K, neither electronic nor vibrational energy of volborthite is available for the energy absorption causing the specific heat anomalies. Thus, in the following, we analyze the dependence of the specific heat anomalies on T and B in terms of the entropy spectra of Group A, B and C (**Figure 4b**).

C. Dependence of the specific heat anomalies on the magnetic entropy spectra

As shown above, the entropy $S_A(2m)$ of Group A is smaller than that of Group B or C by $S_E(2m)$. As the magnetic field B increases from 0, a kagomé layer starts absorbing energy by exploiting the entropy spectrum of Group A, so the anomaly below ~ 4.2 T arises from the entropy spectrum of Group A. Since $\Omega_A(2m)$ becomes larger with increasing $2m$ from 0 to $N/2$ and also with decreasing $2m$ from N to $N/2$, more states are involved in the energy absorption from Zeeman energy. This explains why the intensity of the specific anomaly increases with increasing the field B . The entropies $S_A(2m)$ from the states for $2m = 0 - N/2$ as well as $2m = N - N/2$ are used to

absorb energy, eventually reaching the highest entropy level $S_A(N/2)$ (**Figure 4b**). When all entropy levels are thermally populated, there is no more entropy level with which a kagomé layer can absorb energy any further even if B is increased. At this stage, the spin ladder ordering in a kagomé layer assumes a liquid-like disordered state, and the specific heat in the valley between ~ 4.2 T and ~ 5.5 T reaches that of the disordered state of the $S=1/2$ AUH chains (the green plateau in **Figure 4a**).

When the magnetic field increases further, a kagomé layer can utilize the entropy spectra of Groups B and C to absorb energy further leading to the broad specific heat anomaly above ~ 5.5 T. However, this requires that the spin ladder arrangements of a kagomé layer must be converted from Group A to Groups B and C. Each spin ladder has two sets of J_1 exchanges, e.g., a (AF)-coupled spin ladder has one set of AFM-coupled J_1 and another set of FM-coupled J_1 exchanges. Suppose that a set of J_1 paths is switched from FM to AFM, e.g., from an (AF)-coupled to a (AA)-coupled spin ladder in one member of $\Omega_A(2m)$ of Group A to create an extra (AA)-coupled spin ladder. Such a J_1 -flip, e.g., $(AF)_m(AF)(A/F)_n \rightarrow (AF)_m(AA)(FA)_n$, converts the electronic structure from Group A to Group B, raising the entropy from $S_A(2m)$ to $S_B(2m) = S_A(2m) + S_E(2m)$. Similarly, a J_1 -flip can create an extra (FF)-coupled spin ladder, e.g., $(FA)_m(FA)(FA)_n \rightarrow (FA)_m(FF)(AF)_n$, converting the electronic structure from Group A to Group C, raising the entropy from $S_A(2m)$ to $S_C(2m) = S_A(2m) + S_E(2m)$.

With magnetic fields it is energetically more favorable to induce a J_1 -flip from AFM to FM rather than that from FM to AFM. In contrast, a thermally driven J_1 -flip from AFM to FM would be equally favorable as that from FM to AFM. Thus, thermal energy would be more effective in inducing J_1 -flips than Zeeman energy approximately by a factor of 2. The two specific heat ridges of the below-4.5 T anomaly are nearly parallel to the magnetic field axis, whereas the single

specific heat ridge of the above-5.5 T anomaly is slanted with slope $g\mu_B B/k_B T \approx 2$. This reflects that, when B is strong enough, an increase in B contributes to the energy absorption of each kagomé layer as does that in T , but magnetic field is less effective than thermal agitation in inducing J_1 -flips.

The below-4.5 T anomaly has two specific heat ridges because it consists of both a 2D SRO within kagomé layers and a 3D LRO, while the above-5.5T anomaly has only one broadened specific heat ridge because only 2D SRO is permitted. The entropy spectra of Groups B and C are both involved in the above-5.5T anomaly, but that of only Group A in the below-4.5T anomaly. In terms of electronic structure, all kagomé layers belong to Group A below ~ 4.5 T, whereas each kagomé layer can belong to either Group B or Group C above ~ 5.5 T. This explains why a 3D LRO disappears above ~ 5.5 T.

Finally, it should be pointed out that, in all ordered magnetic states of Groups A – C, there occurs a strong gain of translational entropy with respect to those states in which there is no order between neighboring spin ladders, because the ordered states have translational symmetry along the leg direction. This provides a strong driving force for the magnetic ordering. In a sense, this situation is similar to the nematic phase transition in a system of thin rods examined by Onsager.³⁴

5. Discussion

Our new experimental and theoretical data of the magnetic properties of the kagomé system volborthite reveal that each kagomé layer is partitioned into weakly coupled two-leg spin ladders, which at low temperatures collapse to chains of $S=1/2$ pseudospins. Interactions between adjacent spin ladders in each kagomé layer of volborthite are very weak and are topologically constrained thereby leading to three sets of entropy spectra identical in enthalpy, the occupation of which can

be tuned by an external magnetic field. These three magnetic entropy spectra provide natural explanations for not only the suppression of two-dimensional correlation and magnetic order by a magnetic field of ~ 4.2 T but also the emergence of a new broad specific heat anomaly at magnetic fields above ~ 5.5 T. We argued that the spin ladder arrangements described by the entropy spectrum A allow for an ordering between adjacent kagomé layers, viz., to long-range order. The entropy spectra B and C are identical in the degeneracy of each entropy level, but differ in the nature of spin ladder arrangements. Whether a given kagomé layer produces the entropy spectrum B or C has no effect on the enthalpy difference. Consequently, there is no ordering between kagomé layers, which explains the occurrence of a single specific heat anomaly at magnetic field above ~ 5.5 T. The latter forms a single ridge with increasing B (**Figure 4a**), the shape of which suggests that not all available entropy states of the entropy spectra B and C are populated at 9 T. If the ridge is assumed to have a symmetrical shape as a function of B and T , one might expect that this specific heat anomaly will disappear at magnetic field higher than ~ 13 T. It is highly desirable to measure the specific heat of volborthite under field higher than 9 T. An additional support for the entropy-driven nature of the specific anomalies below 1.5 K comes from the finding that the specific heat anomalies below 1.5 K is hardly affected by the isotope exchange H \rightarrow D unlike the structural phase transition from the $I2/a$ to the $P2_1/a$ structure.

6. Concluding remarks

In conclusion, volborthite is a crystalline magnetic solid with spin exchanges in the kagomé layers of Cu²⁺ ions spread over two orders of magnitude; strong interactions form isolated linear trimers, weaker interactions between linear trimers form two-leg spin ladders with the trimers as effective $S=1/2$ rungs, and then very weak interactions between the spin ladders give rise to a short

range ordering within the kagomé layers. Moderate magnetic fields are sufficient to destroy this spin ladder ordering but higher fields can reconstitute a new spin ladder ordering with higher entropy in the kagomé layers. These unprecedented specific heat anomalies are caused by the three sets of entropy spectra of each kagomé layer, which originate from the topological constraints on the spin ladder ordering in the kagomé layers, and these magnetic field induced transitions are purely entropy-driven.

Acknowledgments

The work at KHU was supported by the Basic Science Research Program through the National Research Foundation of Korea (NRF) funded by the Ministry of Education (2020R1A6A1A03048004).

Competing interests

The authors declare no competing interests.

References

1. P. Mendels and A. S. Wills, in C. Lacroix, P. Mendels, F. Mila, Introduction to Frustrated Magnetism, Springer Series in Solid-State Sciences, 164, Springer, Berlin, Heidelberg, 2011, Balents Savary.
2. S. V. Syzranov and A. P. Ramirez, arXiv:2105.08070.
3. H. J. Xiang, C. Lee, H.-J. Koo, X. Gong, M.-H. Whangbo, Dalton Trans. **42**, 823-853 (2013).
4. M.-H. Whangbo, H. J. Xiang, in *Handbook in Solid State Chemistry, Volume 5: Theoretical Descriptions*, edited by R. Dronskowskii, S. Kikkawa, A. Klein (Wiley, 2017), pp. 285-343.

5. Z. Hiroi, H. Ishikawa, H. Yoshuda, J. Yamamura, Y. Okamoto, *Inorg. Chem.* **58**, 11949-11960 (2019).
6. H. Ishikawa, J. I. Yamaura, Y. Okamoto, H. Yoshida, G. J. Nilsen, Z. Hiroi, *Z. Acta Cryst. C* **68**, i41–i44 (2012).
7. H. Yoshida, J. Yamamura, M. Isobe, Y. Okamoto, G. J. Nielson, Z. Hiroi, *Nat. Commun.* **29**, 860 (2012).
8. H. Ishikawa, M. Yoshida, K. Nawa, M. Jeong, S. Kramer, M. Horvatić, C. Berthier, M. Takigawa, M. Akaki, A. Miyake, M. Tokunaga, K. Kindo, J. Yamaura, Y. Okamoto, Z. Hiroi, *Phys. Rev. Lett.* **114**, 227202 (2015).
9. D. Nakamura, T. Yamashita, H. Ishikawa, Z. Hiroi, S. Takeyama, *Phys. Rev. B* **98**, 020404(R) (2018).
10. S. Yamashita, T. Moriura, Y. Nakazawa, H. Yoshida, Y. Okamoto, and Z. Hiroi, *J. Phys. Soc. Japan* 2010, 79, 083710.
11. O. Janson, S. Furukawa, T. Momoi, P. Sindzingre, J. Richter, K. Held, *Phys. Rev. Lett.* **117**, 037206 (2016).
12. H. W. Yan, Y. Z. Luo, X. Xu, L. He, J. Tan, Z. H. Li, X. F. Hong, P. He, and L. Q. Mai, *ACS Appl. Mater. Interfaces* **9**, 27707–27714 (2017).
13. G. Kresse and J. Furthmüller, *Comput. Mater. Sci.* **6**, 15-50 (1996).
14. G. Kresse and J. Furthmüller, *Phys. Rev. B* **54**, 11169-11186 (1996).
15. G. Kresse and D. Joubert, *Phys. Rev. B* **59**, 1758-1775 (1999).
16. P. E. Blöchl, *Phys. Rev. B* **50**, 17953-17979 (1994).
17. J. P. Perdew, K. Burke, and M. Ernzerhof, *Phys. Rev. Lett.* **77**, 3865 (1996).

18. S. L. Dudarev, G. A. Botton, S. Y. Savrasov, C. J. Humphreys, and A. P. Sutton, *Phys. Rev. B* **57**, 1505 (1998).
19. M.-H. Whangbo, H.-J. Koo, and R. K. Kremer, *Molecules*, **26**, 531(2021).
20. D. C. Johnston, R. K. Kremer, M. Troyer, X. Wang, A. Klümper, L. Bud'ko, A. F. Panchula, P. C. Canfield, *Phys. Rev. B* **61**, 9558-9606 (2000).
21. P. W. Selwood, *Magnetochemistry* (Interscience Publishers Inc., New York 1956).
22. G. A. Bain, J. F. Berry, *J. Chem. Educ.* **85**, 532 – 536 (2008).
23. M. G. Banks, R. K. Kremer, C. Hoch, A. Simon, B. Ouladdiaf, J.-M. Broto, H. Rakoto, C. Lee, M.-H. Whangbo, *Phys. Rev. B* **80**, 024404 (2009).
24. A. Abragam, B. Bleaney, *Electron Paramagnetic Resonance of Transition Ions* (Oxford University Press, New York, 1970).
25. A. Boukhari, A. Moquine, and S. Flandrois, *Mat. Res. Bull.* **21**, 395 (1986).
26. S. Todo, K. Kato, *Phys. Rev. Lett.* **87**, 047203 (2001).
27. A. F. Albuquerque, A. Fabien, P. Corboz, et al. *J. Magn. Magn. Mater.* **310**, 1187-1193 (2007).
28. P. Y. Zavalij, Fan Zhano, and M. S. Whittingham, *Acta Cryst.* **1997**, C53, 1738–1739.
29. W. O. J. Boo and J. W. Stout, *J. Chem. Phys.* **1979**, 71, 9–16.
30. D. Frenkel, *Physica A* **263**, 26-38 (1999).
31. N. Ch. Karayiannis, K. Foteinopoulou, and M. Laso, *Phys. Rev. Lett.* **103**, 045703 (2009).
32. M. A. Boles, M. Engel, and D. Talapin, *Chem. Rev.* **116**, 11220-11289 (2016).
33. P. Damasceno, M. Engel, and S. C. Glotzer, *Science* **337**, 453-457 (2012)
34. L. Onsager, *Proc. Annals NY. Acad. Sci.* **51**, 627-659 (1949).
35. B. Amadon, S. Biermann, A. Georges, and F. Ariasetiawan, *Phys. Rev. Lett.* **96**, 066402 (2006).

36. T. Chen, B. J. Foley, C. Park, C. M. Brown, L. W. Harriger, J. Lee, J. Ruff, M. Yoon, J. J. Choi, and S.-H. Lee, *Sci. Adv.* **2**, e1601650 (2016).

Supplementary Material

for

Purely entropy-driven magnetic phase transitions in the kagomé system volborthite

Myung-Hwan Whangbo^{a,b,*}, Hyun-Joo Koo^b, Eva Brücher^c, Pascal Pupal^c, and Reinhard K. Kremer^{c,*}

^a Department of Chemistry, North Carolina State University, Raleigh, NC 27695-8204, USA

^b Department of Chemistry and Research Institute for Basic Sciences, Kyung Hee University, Seoul 02447, Republic of Korea

^c Max Planck Institute for Solid State Research, Heisenbergstrasse 1, D-70569 Stuttgart, Germany

Spin exchanges of the $I2/a$ and $P2_1/a$ phases of volborthite by energy mapping analysis

To extract the values of the spin exchanges for the $I2/a$ and $P2_1/a$ phases of volborthite, we carry out DFT calculations encoded in the VASP^{1,2} using the augmented plane wave method^{3,4} and the PBE exchange-correlation functional.⁵ To take into account the effect of electron correlation of the Cu 3d states, we use the DFT plus on site repulsion (DFT+U) method⁶ with $U_{\text{eff}} = U - J = 4$ and 5 eV.

A. $I2/a$ phase

To determine the five spin exchanges $J_1 - J_5$ of the $I2/a$ phase, we consider six ordered spin states FM, AF(i) ($i = 1$ to 5) shown in **Figure S1**. Then, the total spin exchange energies of these states can be written as

$$E = \sum_{i=1}^5 n_i J_i S^2 \quad (\text{S1})$$

where S refers to the spin of the Cu^{2+} ion (i.e., $S = 1/2$). The values of n_i ($i = 1$ to 5) found for the six spin states are listed in **Table S1**. The relative energies (meV/FU) obtained for the FM, and AF*i* ($i = 1 - 5$) states by DFT+U calculations are listed in **Table S2**. By mapping the relative energies of the ordered magnetic states determined by DFT+U calculations to those determined by the spin exchange energies, we obtain the values of the spin exchanges $J_1 - J_5$ listed in **Table S3** and **Table 1** of the text.

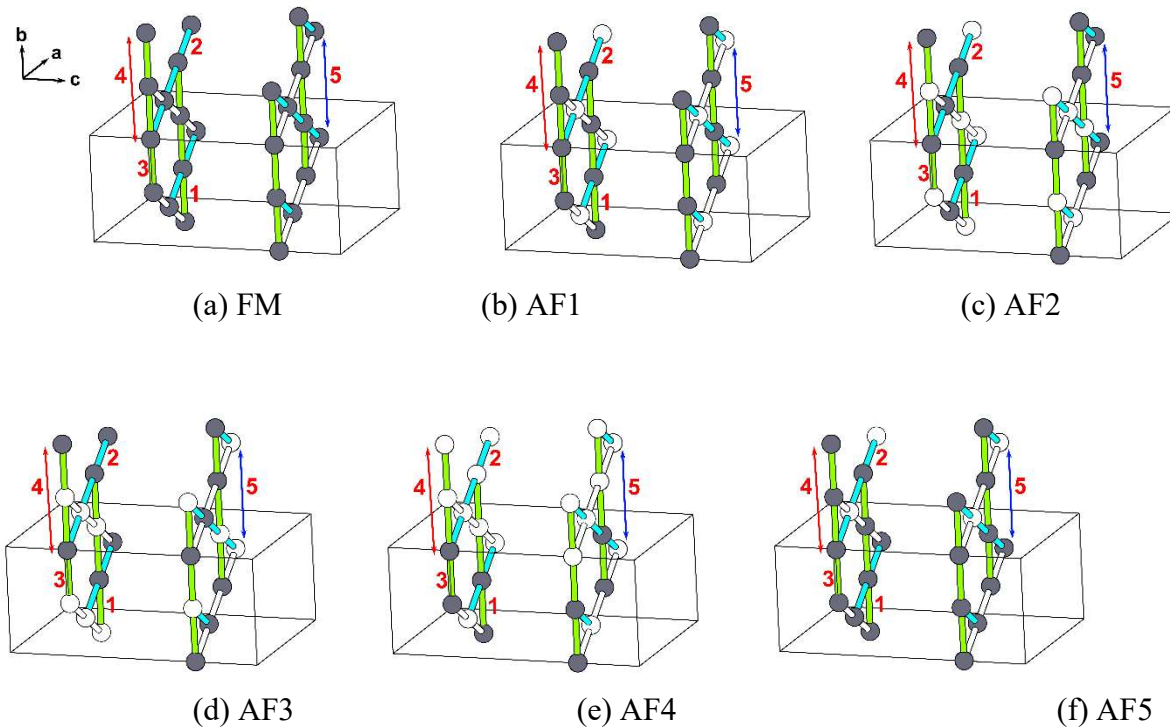


Figure S1. Six ordered spin states, i.e., the FM and AF(i) ($i = 1$ to 5) states, of the $I2/a$ phase employed for the energy-mapping analysis, where the gray and white circles represent the up and down spin sites of Cu^{2+} ions.

Table S1. Values of n_i for the six ordered spin states

	n_1	n_2	n_3	n_4	n_5
E_{FM}	-16	-16	-16	-16	-8
E_{AF1}	16	16	-16	-16	-8
E_{AF2}	-16	16	16	-16	-8
E_{AF3}	16	-16	16	-16	-8
E_{AF4}	0	0	0	16	-8
E_{AF5}	0	0	-16	-16	8

Table S2. Relative energies (meV/FU) obtained from DFT+U calculations

	$U_{\text{eff}} = 4 \text{ eV}$	$U_{\text{eff}} = 5 \text{ eV}$
FM	47.87	37.85
AF1	0.69	0
AF2	0	0.65
AF3	46.24	38.49
AF4	16.94	13.61
AF5	23.95	18.63

Table S3. Values of the spin exchanges $J_1 - J_5$ (in K) calculated for the $I2/a$ phase

	$U_{\text{eff}} = 4 \text{ eV}$	$U_{\text{eff}} = 5 \text{ eV}$
J_1/J_2	0.010	0
J_3/J_2	0.025	-0.017
J_4/J_2	0.145	0.149
J_5/J_2	0.014	0.016
J_2	542 K	439 K

B. $P2_1/a$ phase

To determine the 10 spin exchanges of the $P2_1/a$ phase, namely, $J_1 - J_5$ for the layer 1 and $J'_1 - J'_5$ for the layer 2, we consider 11 ordered spin states FM, AF(i) ($i = 1$ to 10) shown in **Figure S2**. Then, the total spin exchange energies of these states can be written as

$$E = \sum_{i=1}^5 n_i J_i S^2 + \sum_{i=1}^5 n'_i J'_i S^2 \quad (\text{S2})$$

where $S = 1/2$. The values of n_i ($i = 1$ to 5) and n'_i ($i = 1$ to 5) found for the 11 spin states are listed in **Table S4**. The relative energies (meV/FU) obtained for the FM, and AFi ($i = 1 - 10$) states by DFT+U calculations are listed in **Table S5**. By mapping the relative energies of the ordered magnetic states determined by DFT+U calculations to those determined by the spin exchange energies, we obtain the values of the spin exchanges listed in **Table S6** and **Table 1** of the text.

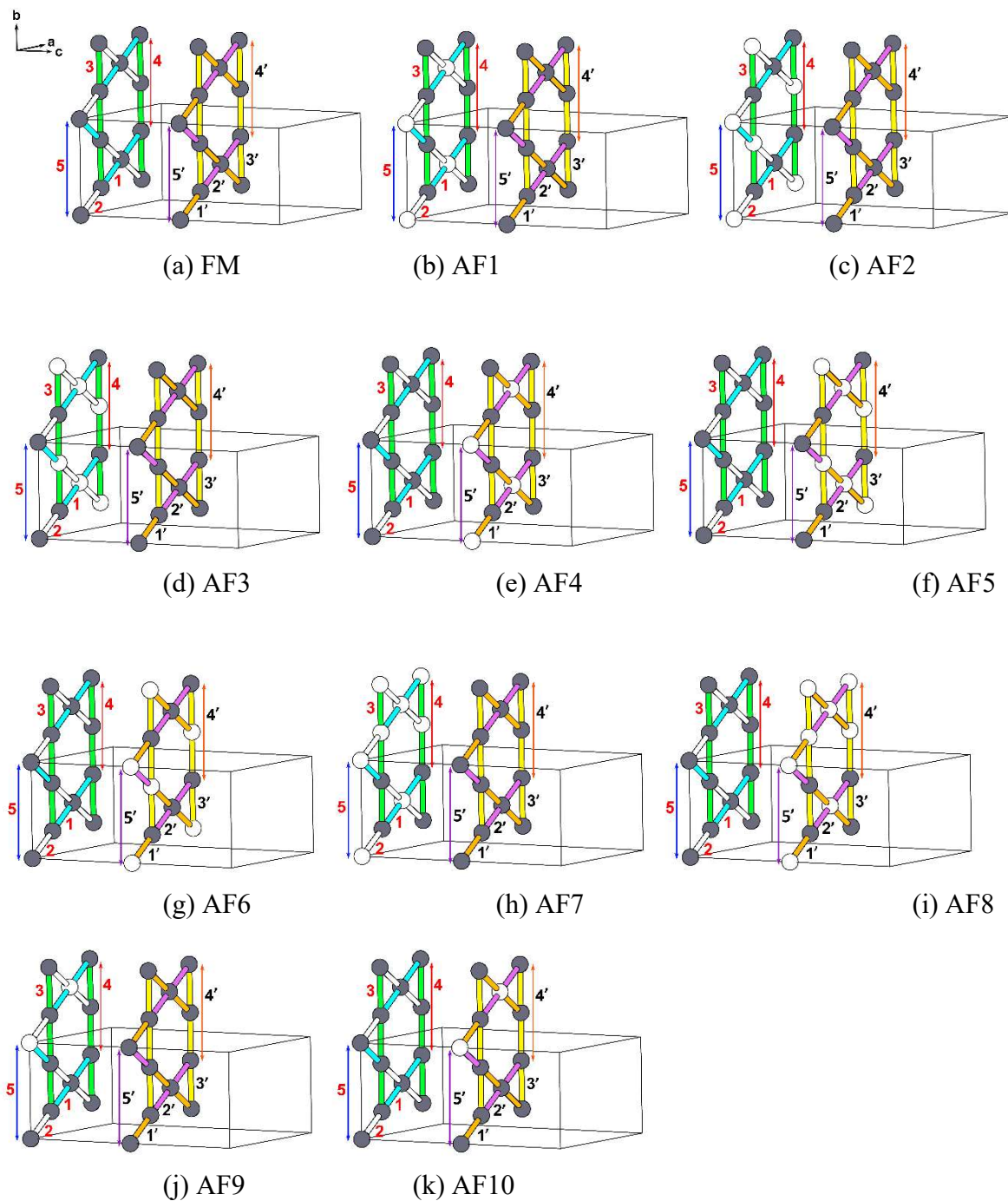


Figure S2. 11 ordered spin states, i.e., the FM and AF(i) ($i = 1$ to 10) states, of the $P2_1/a$ phase employed for the energy-mapping analysis, where the gray and white circles represent the up and down spin sites of Cu^{2+} ions.

Table S4. Values of n_i and n_i' for the 11 ordered spin states

	n_1	n_2	n_3	n_4	n_5	n_1'	n_2'	n_3'	n_4'	n_5'
E_{FM}	-8	-8	-8	-8	-4	-8	-8	-8	-8	-4
E_{AF1}	8	8	-8	-8	-4	-8	-8	-8	-8	-4
E_{AF2}	-8	8	8	-8	-4	-8	-8	-8	-8	-4
E_{AF3}	8	-8	8	-8	-4	-8	-8	-8	-8	-4
E_{AF4}	-8	-8	-8	-8	-4	8	8	-8	-8	-4
E_{AF5}	-8	-8	-8	-8	-4	-8	8	8	-8	-4
E_{AF6}	-8	-8	-8	-8	-4	8	-8	8	-8	-4
E_{AF7}	0	0	0	8	-4	-8	-8	-8	-8	-4
E_{AF8}	-8	-8	-8	-8	-4	0	0	0	8	-4
E_{AF9}	0	0	-8	-8	4	-8	-8	-8	-8	-4
E_{AF10}	-8	-8	-8	-8	-4	0	0	-8	-8	4

Table S5. Relative energies (meV/FU) obtained from DFT+U calculations

	$U_{\text{eff}} = 4 \text{ eV}$	$U_{\text{eff}} = 5 \text{ eV}$
FM	25.87	20.25
AF1	2.18	1.21
AF2	1.42	1.21
AF3	25.14	20.61
AF4	1.41	0.58
AF5	0	0
AF6	25.72	21.08
AF7	10.31	8.03
AF8	9.86	7.65
AF9	13.86	10.59
AF10	13.49	10.27

Table S6. Values of the spin exchanges $J_1 - J_5$ (in K) calculated for the $P2_1/a$ phase

	$U_{\text{eff}} = 4 \text{ eV}$		$U_{\text{eff}} = 5 \text{ eV}$	
	Layer 1	Layer 2	Layer 1	Layer 2
J_1/J_2	-0.001	-0.025	-0.009	-0.035
J_3/J_2	0.031	0.031	-0.009	-0.006
J_4/J_2	0.141	0.135	0.145	0.138
J_5/J_2	0.014	0.013	0.015	0.014
J_2	550 K	582 K	446 K	473 K

References

1. G. Kresse, J. Furthmüller, *Comput. Mater. Sci.* **6**, 15-50 (1996).
2. G. Kresse, J. Furthmüller, *Phys. Rev. B* **54**, 11169-11186 (1996).
3. G. Kresse, D. Joubert, *Phys. Rev. B* **59**, 1758-1775 (1999).
4. P. E. Blöchl, *Phys. Rev. B* **50**, 17953-17979 (1994).
5. J. P. Perdew, K. Burke, M. Ernzerhof, *Phys. Rev. Lett.* **77**, 3865 (1996).
6. S. L. Dudarev, G. A. Botton, S. Y. Savrasov, C. J. Humphreys, A. P. Sutton, *Phys. Rev. B* **57**, 1505-1509 (1998).